- **Building volumes** modeling rules:
  1. A **space air volume** is modeled by **a single capacitor (1C)**.
  2. The **outside air volume** is modeled by an **AC voltage source (AC)**, as its temperature changes with respect to time.
  3. The **ground volume** attached to the building is modeled by a **DC source (DC)**, as its temperature remains constant over a long period of time.
- **Node** assignment rules:
  1. **Network nodes** which include: inner or outer surface nodes $su_i, su_o \in$ Su (Su is the set of surface node indexes) assigned to building constructions, air volume nodes $sp_i \in$ Sp (Sp is the set of space node indexes), assigned to building spaces.
  2. Two **boundary nodes** are also assigned: the first is assigned to the outside air volume (outside air node), and the second to the ground volume attached to the building (ground node).

SRC uses the RC-Network representation in order to populate:

- A **conductance matrix** $[R_t]$ containing all the thermal resistances populated according to their interconnections.
- A **capacitance matrix** $[C_t]$ which is a diagonal matrix containing all the thermal capacitors of the building elements.
- A **heat flow rate vector** Q_t.

Q_t contains all the heat flow rates at the RC-Network nodes, which are updated by:

- **Solar heat flow rates** on surface nodes $su \in$ Su: $\mathbf{\Delta Q^{sol}(su)}$ (ASHRAE (2007), Perez et al. (1990)) which involve shading calculations using shade projection (Vatti, B.R. (1992)). Solar radiation passing from openings to building interior spaces, is evaluated using the solar heat gain coefficients of the openings for different incident angles.
- **Long-wave radiation (LWR) heat flow rates** on surface nodes $su \in$ Su: $\mathbf{\Delta Q^{LWR}(su)}$ (View factors calculation: Winget, J.M. et. al. (1989), LWR on internal surfaces: Oppenheim (1956), LWR on external surfaces: Cole (1976)). The long wave radiation from the openings to the internal walls is calculated using the view factor pairs of the openings with the respective walls.
- **Heat flow rates from boundary nodes** on surface nodes $su \in$ Su: $\mathbf{\Delta Q^{air}(su)}$ (outside air) and $\mathbf{\Delta Q^{gnd}(su)}$ (ground).
- **Micro-climate devices' heat flow rates** to space nodes $sp \in$ Sp: $\mathbf{\Delta Q^{dev}(sp)}$ (openings, blinds, heaters, HVACs, air conditioners,... ASHRAE (2009b)) .
- **Infiltration heat flow rates** to space nodes $sp \in$ Sp: $\mathbf{\Delta Q^{inf}(sp)}$ ASHRAE (2009b).
- **Internal gains' heat flow rates** to space nodes, $sp \in$ Sp: $\mathbf{\Delta Q^{ig}(sp)}$ and associated internal surfaces, $su_i \in$ Su: $\mathbf{\Delta Q^{ig}(su)}$ ASHRAE (2009b).

The time evolution of the temperatures at the RC-Network nodes, included in vector T_t, can be described by a system of ODEs involving the $[C_t]$ and $[R_t]$ matrices and the Q_t vector, formed according to the Kirchhoff current laws for electrical circuits:

$$[C_t]\frac{dT_t}{dt} = [R_t]T_t + Q_t \quad (1)$$

1.2.2 H-Network

In SRC the air volumes of building spaces together with the outside air volume encompassing the building under consideration, are assumed to interchange water vapor quantities. The concentration of water vapor in each air volume, is measured using the humidity ratio measure (ASHRAE (2009a)). The building air volumes are represented by network nodes and the water vapor flow paths by network edges, forming a humidity network called H-Network. H-Network conforms with the following node and edge assignment rules:

1. **Network nodes** are assigned to the **air volumes of building spaces** (inside air volume nodes).
2. **A single boundary node** is assigned to the **outside air volume** (outside air volume node).
3. **Edges** connecting the H-Network nodes are assigned to **humidity flow paths**, which are associated with air flows between building air volumes. Air flows are realized at the locations of, either external building openings (connecting outside with inside air volume nodes), or internal building openings (connecting internal air volume nodes), or at the locations of mechanical ventilation devices (HVACs, fans,...).

H-Network is used in order to form:

- The **dry air mass matrix** $[M_t]$ which is a diagonal matrix with dimension equal to the number of building spaces containing at entry $M_t(sp_i, sp_i)$ the mass of dry air of air volume of space $sp_i \in$Sp.
- The **water-vapor rate vector** W_t which contains at entry sp_i the total incoming water vapor mass rate to the air volume of space sp_i:

$$W_t(sp_i) = \sum_{sp_k \in N_{sp_i}} w_t(sp_k, sp_i) \quad (2)$$

N_{sp_i} is the set of neighbor nodes to node sp_i. Neighbor nodes of sp_i are the nodes connected with humidity flow paths to node sp_i. $w_t(sp_k, sp_i)$ is the water vapor mass flow rate from node sp_k to node sp_i. Vapor mass flows

are generated during the operation of microclimate devices (HVACs, openings ...) , which transfer air masses either from outside or neighbor spaces sp_k, to space sp_i.

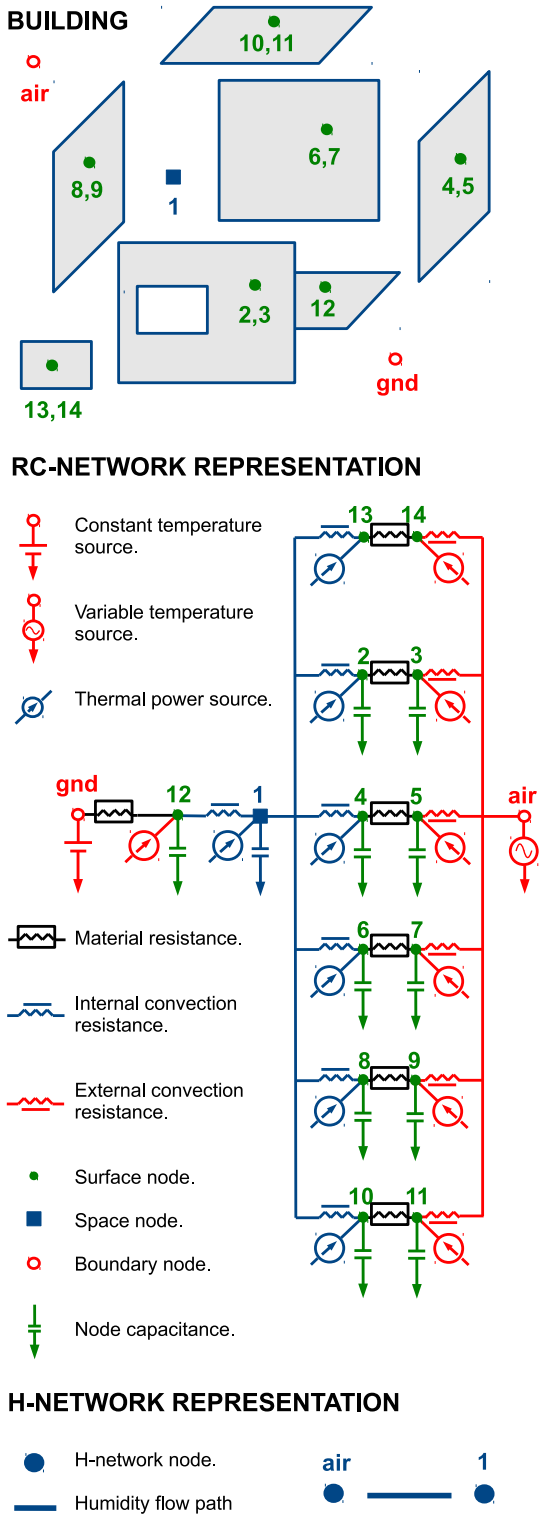

Figure 2: RC and H Network building representations

The time evolution of the humidity ratio values, referring to the air-volumes of the building spaces (included in vector H_t), can be described by a system of ODEs, involving the $[M_t]$ matrix and the W_t vector, according to the water vapor mass conservation law below water vapor saturation levels:

$$[M_t]\frac{dH_t}{dt} = W_t \tag{3}$$

1.3 Numerical scheme

SRC follows a first order and forward difference numerical scheme of variable time step. The variable time step is selected in order to preserve small variances among consecutive temperature results and execution speed. Although necessary conditions for stability of the scheme have not been established, due to the mathematical complexity of the underlying model, a temperature variance rule is introduced which preserved stability in the results of all of the tested scenarios. Additionally, the first order of the scheme is selected in order to: enable the formation of time varying linear systems, describing the thermal behavior of the whole building (such as (14)), and facilitate model based temperature control schemes, highlighting SRC's contribution. SRC's numerical calculations at time instances $f \in \{1, ..., F\}$, can be summarized by the following steps:

1. An initial temperature profile for the temperatures at the RC-network nodes (contained in vector T_0), an initial humidity ratio profile, referring to the humidity ratio values at the H-network nodes (contained in vector H_0) and an initial time step δt_0, are considered.
2. The heat flow rates at every building space node $sp_i \in$ Sp, are updated by adding the total heat flow rate to node sp_i at time f ($\Delta Q_f(sp_i)$):

$$Q_f(sp_i) \rightarrow Q_{f-1}(sp_i) + \Delta Q_f(sp_i) \tag{4}$$

The total heat flow rate at sp_i, is given by:

$$\Delta Q_f(sp_i) = \sum_{sp_k \in N_{sp_i}} \rho_f^{air}(sp_k)\dot{V}_f(sp_k, sp_i)\Delta h_f(sp_k, sp_i) \tag{5}$$

N_{sp_i} is the set of neighbor air volumes to air volume sp_i. $\dot{V}_f(sp_k, sp_i)$ is the air transfer rate from volume of space sp_k to volume of space sp_i, $\rho_f^{air}(sp_k)$ is the density of air in volume sp_k and $\Delta h_f(sp_k, sp_i) = h_f(sp_k) - h_f(sp_i)$ is the enthalpy change with $h_f(sp_k)$, $h_f(sp_i)$ being the enthalpies of air volumes of spaces sp_k and sp_i. The enthalpy of air volume of space sp_i, at time instant f is calculated by:

$$h_f(sp_i) = [c_{p,da} + c_{p,w}H_f(sp_i)]\,T_f(sp_i) \tag{6}$$

where $c_{p,da}$ and $c_{p,w}$ are the specific heats of dry air and water vapor respectively and $T_f(sp_i)$ is the dry bulb temperature of air volume of space sp_i, at time instant f.

3. Similarly, the heat flow rate at every building surface node $su \in$ Su, is updated by adding the total heat flow rate to node su, $\Delta Q_f(su)$:

$$Q_f(su) \rightarrow Q_{f-1}(su) + \Delta Q_f(su) \quad (7)$$

4. The future temperature estimates (contained in vector T_{f+1}), are evaluated using the current time step dt_f, the present values T_f, and a finite differences forward numerical scheme on (1), at time instance f:

$$T_{f+1} = [A_f]T_f + \bar{Q}_f \quad (8)$$

where: $[A_f]$ is the transition matrix:

$$[A_f] = I + \delta t_f [C_f]^{-1}[R_f] \quad (9)$$

($[R_f]$, $[C_f]$ are the time samples of $[R_t]$ and $[C_t]$ matrices) and $\bar{Q}_f$ is the reduced heat flow rate vector:

$$\bar{Q}_f = \delta t_f [C_f]^{-1} Q_f \quad (10)$$

Q_f is the heat flow rate vector, updated in the previous steps.

5. Similarly, using the humidity mass transfer ODE: (3), and the current humidity ratio values H_f, the future humidity ratio estimates of building spaces H_{f+1}, are approximated using the following expressions:

- **Humidity below saturation levels**
  $(H_f(sp) < H_{sat}(sp) \vee L_f(sp) \leq 0)$
  $H_{f+1}(sp) = H_f(sp) + \delta t_f [M_f(sp)]^{-1} W_f(sp)$
  $L_{f+1}(sp) = 0$
- **Humidity above saturation levels**
  $(H_f(sp) \geq H_{sat}(sp) \vee L_f(sp) > 0)$
  $H_{f+1}(sp) = H_{sat}(sp)$
  $L_{f+1}(sp) = L_f(sp) + \delta t_f [M_f(sp)]^{-1} W_f(sp)$ (11)

As in case of the thermal ODE, $[M_f(sp)]$ and $W_f(sp)$ are samples of the dry air mass matrix $[M_t(sp)]$ and air-vapor flow rate vector $W_t(sp)$, of space sp's air volume at time instant f. $L_f(sp)$ and $L_{f+1}(sp)$ are the liquified vapor vectors at time instances f and $f+1$, containing the fraction of the total air mass which the vapor quantities occupy and turn into liquid in space sp. Although the last case of (11) was not used in the simulation examples, as saturation conditions never satisfied, it is required in order to preserve the humidity mass equilibrium and it will be added for completeness in the future.

6. Finally, in order to avoid large temperature variances, the maximum value of the absolute difference between the future and present temperature vectors: $\max(|\Delta T_{f+1}|) = \max(|T_{f+1} - T_f|)$, is compared against a temperature sensitivity value (T_{sens}) and some of the simulation parameters are updated according to the following temperature variance rule:

- **Small temperature variance**
  $(\max(|\Delta T_{f+1}|) \leq T_{sens})$

$$\begin{cases} \delta t_{f+1} = \delta t_f \\ \{T_f, H_f\} = \{T_{f+1}, H_{f+1}\} \\ f \rightarrow f+1 \end{cases} \quad (12)$$

- **Large temperature variance**
  $(\max(|\Delta T_{f+1}|) > T_{sens})$

$$\begin{cases} \delta t_{f+1} = \frac{\delta t_f}{2} \\ \{T_f, H_f\} = \{T_{f-1}, H_{f-1}\} \end{cases} \quad (13)$$

For all the simulations presented here the temperature sensitivity value was set at $T_{sens} = 0.1^o$C.

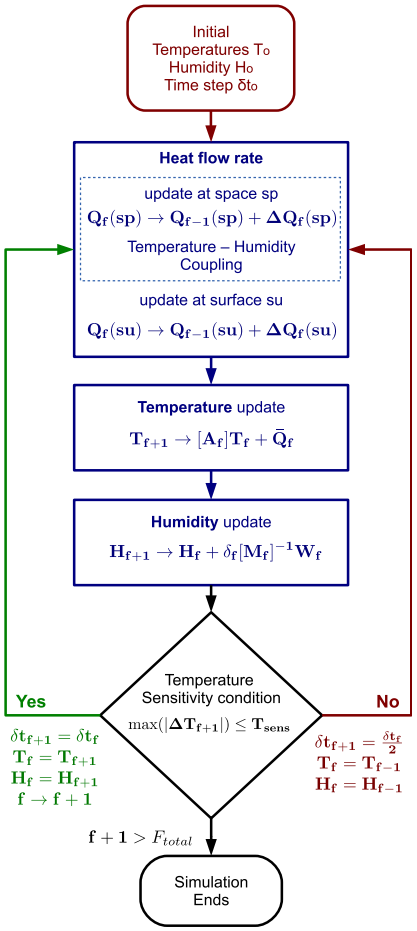

Figure 3: Numerical scheme of SRC

1.4 Contribution

The development of SRC was motivated by the need of a consistent systemic representation of a building, where the time evolution of temperatures of the building elements, satisfy a "global" linear system of equations derived using induction on system (8):

$$\begin{bmatrix} T_1 \\ T_2 \\ \dots \\ T_F \end{bmatrix} = \begin{bmatrix} A_0 & I & 0 & \dots \\ A_1 A_0 & A_0 & I & \dots \\ \dots & \dots & \dots & \dots \\ A_{F-1} \dots A_0 & \dots & \dots & I \end{bmatrix} \begin{bmatrix} T_0 \\ \bar{Q}_0 \\ \dots \\ \bar{Q}_F \end{bmatrix}$$

The compound matrix in the previous relation describes the thermal response of the building, at time instances $\{1, ..., F\}$. The above expression allows climate control methods to be carried out as convex optimization problems, Lilis et al. (2013), where the variables to be controlled (space temperatures for example), are extracted from the global system, forming a smaller system:

$$T(sp) = [A(sp, :)]\bar{Q}(sp) + T_{oth}(sp) \quad (14)$$

Vectors $T(sp) = \{T_1(sp), ..., T_F(sp)\}$ and $\bar{Q}(sp) = \{\bar{Q}_1(sp), ..., \bar{Q}_F(sp)\}$ are the parts of the temperature and heat flow rate vectors, referring to building space nodes. Similarly, $[A(sp, :)]$ contains the rows of the compound matrix which refer to the space nodes. $T_{oth}(sp)$ is the part of $T(sp)$ which depends on the components of $\bar{Q}$ which do not include the space components $\bar{Q}(sp)$, and the initial temperature vector T_o.

1.5 Applications to model based climate control

SRC's mathematical foundation expressed by the subsystem (14) enables the formulation of climate control problems as regularized convex optimization problems Lilis et al. (2013). In such problems the goal is to determine the reduced heat flow rates at building spaces which bring the space temperatures (according to (14)), as close as possible (in the l2-norm sense), to a desired space temperature vector T_d. Mathematically the above are summarized by the following expression:

$$\bar{Q}^*(sp) = \underset{\bar{Q}(sp)}{\arg\min} ||T(sp) - T_d||_2 + \alpha ||\bar{Q}(sp)||_2 \quad (15)$$

The regularization parameter $\alpha > 0$ penalizes the energy demand expressed by $\bar{Q}(sp)$.

EVALUATION CASES

1.6 Case buildings

SRC is tested on **IEA-BESTEST** building cases Neymark et al. (2008), which include a series of buildings named "Case X" ($X = \{195, ..., 320\}$) with geometries displayed in figure 4. The openings, shades, internal gains, infiltration and set points, as well as the radiation absorption coefficients of materials, vary from one building case to another, as displayed in table 4.
Initially two basic building cases are considered: **Case600** characterized by low thermal mass materials and **Case900** which has high thermal mass materials. These cases are simulated assuming no climate control (**Free float cases - FF**) and perfect climate control preserving the internal space temperature within the set points of table 4 (**Loaded cases - LD**).
The second set of simulation scenarios includes the cases **Case195** - **Case320** and more precisely their loaded scenarios. These simulations are performed in order to demonstrate SRC's ability to capture different heat transfer phenomena. This is done by looking at the differences in the annual demands for heating and cooling according to table 3. These annual demands, which refer to each building case, are obtained by calculating the total required energy of ideal devices of infinite capacity, which preserve the internal space temperature at the set point limits of table 4. Significant differences in these demands indicate that the phenomenon under consideration is taken into account during the simulation procedure.

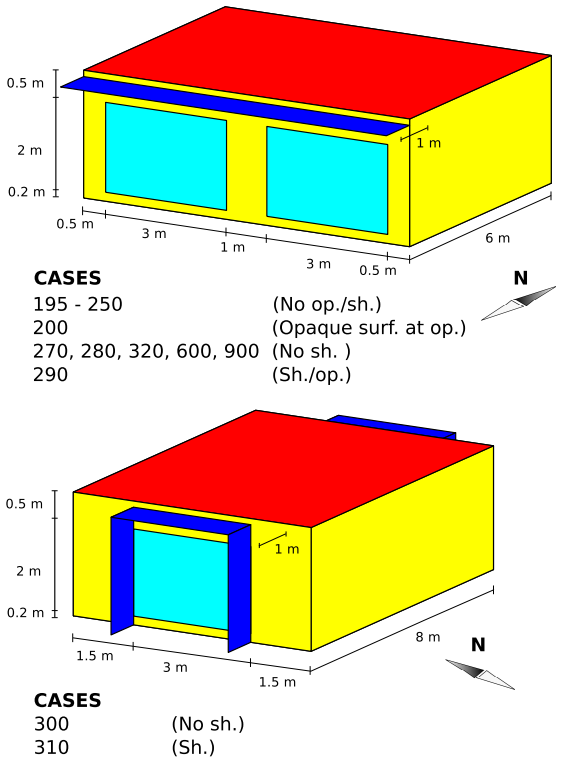

Figure 4: Case buildings' geometries
***op.**: Openings, **sh.**: Shades*

1.7 Comparison

The plots of figures 5 indicate that the annual energy demands for heating and cooling estimated by SRC for the Case 600 (Low thermal mass case, H: 4.61 MWh / C: 7.03 MWh) and Case 900 (High thermal mass case, H: 1.3 MWh / C: 2.62 MWh), are inside the min/max range of BESTEST simulation test programs (BESTEST limits for **Case 600:** Heating 4.296 - 5.709 MWh, Cooling 6.137 - 7.964 MWh, **Case 900:** Heating 1.170 - 2.041 MWh, Cooling 2.132 - 3.415 MWh).

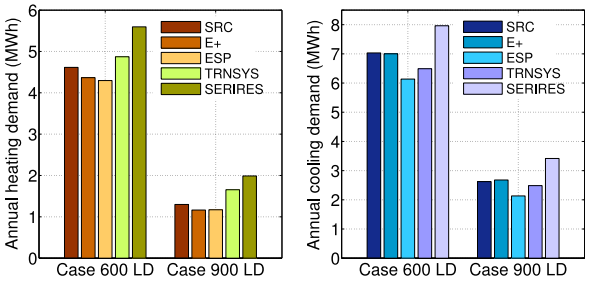

Figure 5: Annual heating and cooling demands for Case 600 (Low mass) and Case 900 (High mass)

Tables 1 and 2 demonstrate that the minimum, maximum and average estimated zone temperatures by SRC are close to the ones estimated by other simulation programs.

Table 1: Maximum - Minimum annual zone temperatures ^oC

Case	600FF min-max	900FF min-max
E+	(-18.07) - (66.00)	(-2.4) - (43.7)
ESP	(-15.60) - (64.90)	(-1.6) - (41.8)
TRNSYS	(-17.80) - (65.30)	(-6.4) - (42.5)
SERIRES	(-10.00) - (69.80)	(-3.9) - (43.4)
SRC	**(-19.11) - (67.34)**	**(-5.87) - (43.16)**

Table 2: Average annual zone temperature ^oC

Case	600 FF	900 FF
E+	26.2	26.4
ESP	25.1	25.5
TRNSYS	24.5	24.5
SERIRES	25.9	25.7
SRC	**25.45**	**25.20**

Finally, the demand differences (displayed in the plots of figure 7) validate that all the phenomena of table 3 are taken into account by SRC and that the obtained demand differences are close to the ones obtained by EnergyPlus.

Table 3: IEA-BESTEST case differences

Case diff.	**Phenomenon under examination**
(195)	Solid conduction
(200)-(195)	Film convection
(210)-(200)	**Ext**ernal IR with internal IR off
(220)-(215)	**Ext**ernal IR with internal IR on
(215)-(200)	**Int**ernal IR with external IR off
(220)-(210)	**Int**ernal IR with external IR on
(230)-(**220**)	Infiltration (Inf.)
(240)-(**220**)	Internal gains (Ig.)
(250)-(**220**)	Exterior solar absorbtance
(270)-(**220**)	South solar transmittance
(280)-(**270**)	Cavity albedo
(290)-(**270**)	South horizontal overhang
(300)-(**270**)	East, west solar transmittance.
(310)-(300)	East, west overhang and fins.
(320)-(**270**)	Thermostat deadband.

CONCLUSIONS

It was demonstrated using the **IEA-BESTEST** diagnostic procedure that, System of Resistances and Capacitances (**SRC**), a new building thermal simulation program, is capable of capturing a variety of phenomena appearing in buildings, which involve: building spaces, internal/external surfaces, as well as microclimate devices (openings, blinds, HVACs,...). These phenomena include: thermal conduction and convection, short-wave (solar) and long-wave (infrared) radiation and humidity mass transfer.
The component-based structure of SRC allows certain tasks to be executed independently (view-factor and solar gain calculations) only once for every building, without requiring to be repeated for each future simulation call, fact that reduces the total simulation time.
Additionally the systemic approach of SRC, offers the ability of forming a global system of linear equations describing the thermal response of the whole building over a finite set of time instances $\{1, ..., F\}$, fact that opens new opportunities to develop state-space based thermal control techniques.

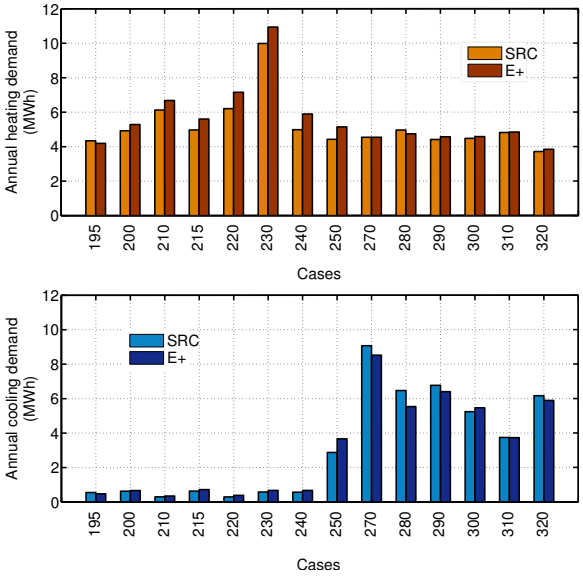

Figure 6: Total heating and cooling demands

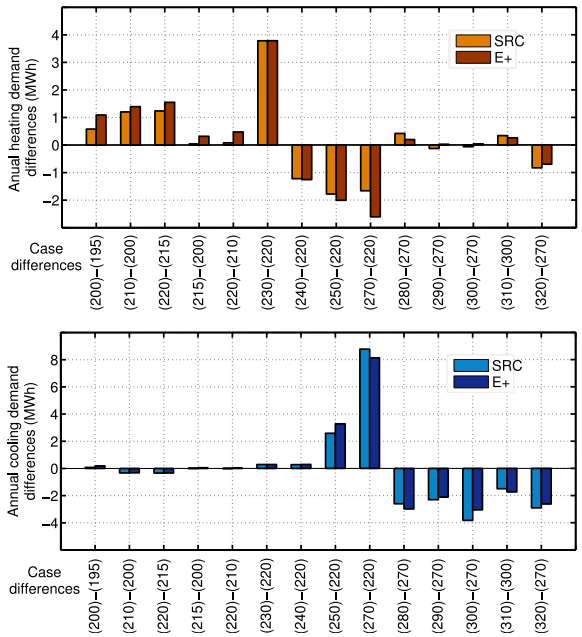

Figure 7: Heating and cooling demand differences

ACKNOWLEDGMENTS

The developement of SRC is supported by the European Commission under contracts PEBBLE: FP7-ICT-

2007-9.6.3 (www.pebble-fp7.eu) and BaaS: FP7-ICT-2011.6.2 (www.baas-project.eu).

Table 4: IEA-BESTEST cases specification.
***Op.** : Opening.*
***G. S.** : Glass Surface.*
***Sh.**: Shade.*
***Ig.P.** : Internal gains power.*
***Inf.**: Infiltration in ACH.*
***Ex.S.** : External shortwave absorption coefficient.*
***Int.S.** : Internal shortwave absorption coefficient.*
***IR.** : Infra-red (longwave) absorption coefficient.*
***Set P.** : Set Points.*
S : South orientation. / E/W : East/West orientation.

Case	Op.	G.S.	Sh.	Ig.P.	Inf.
195	n/a	0	n/a	n/a	n/a
200	n/a	0	n/a	n/a	n/a
210	n/a	0	n/a	n/a	n/a
215	n/a	0	n/a	n/a	n/a
220	**n/a**	**0**	**n/a**	**n/a**	**n/a**
230	n/a	0	n/a	n/a	1
240	n/a	0	n/a	200 W	n/a
250	n/a	0	n/a	n/a	n/a
270	**S**	**12**	**n/a**	**n/a**	**n/a**
280	S	12	n/a	n/a	n/a
290	n/a	12	S	n/a	n/a
300	E/W	6/6	n/a	n/a	n/a
310	E/W	6/6	E/W	n/a	n/a
320	S	12	n/a	n/a	n/a
600	S	12	n/a	200 W	0.5
900	S	12	n/a	200 W	0.5

Case	Ex.S.	In.S.	Ex.IR.	In.IR.	Set P.
195	0.1	n/a	0.1	0.1	20/20
200	0.1	n/a	0.1	0.1	20/20
210	0.1	n/a	0.9	0.1	20/20
215	0.1	n/a	0.1	0.9	20/20
220	**0.1**	**n/a**	**0.9**	**0.9**	**20/20**
230	0.1	n/a	0.9	0.9	20/20
240	0.1	n/a	0.9	0.9	20/20
250	0.9	n/a	0.9	0.9	20/20
270	**0.1**	**0.9**	**0.9**	**0.9**	**20/20**
280	0.1	0.1	0.9	0.9	20/20
290	0.1	0.9	0.9	0.9	20/20
300	0.1	0.9	0.9	0.9	20/20
310	0.1	0.9	0.9	0.9	20/20
320	0.1	0.9	0.9	0.9	20/27
600	0.6	0.6	0.9	0.9	20/27
900	0.6	0.6	0.9	0.9	20/27

REFERENCES

ASHRAE 2007. Solar energy use. *ASHRAE Handbook - HVAC Applications (SI)*, 33:5–6.

ASHRAE 2009a. Psychrometrics. *ASHRAE Handbook - Fundamentals (SI)*, 1:1–16.

ASHRAE 2009b. Ventilation and infiltration. *ASHRAE Handbook*, 16:1–36.

Boyer, H., Chabriat, J., Grondin-Perez, B., Tourrand, C., and Brau, J. 1996. Thermal building simulation and computer generation of nodal models. *Building and environment*, 31(3):207–214.

Cole, R. 1976. The longwave radiation incident upon the external surface of buildings. *Building Services Engineer*, 44:195–206.

Crawley, D., Hand, J., Kummert, M., and Griffith, B. 2008. Contrasting the capabilities of building energy performance simulation programs. *Building and Environment*, 43(4):661–673.

Felgner, F., Agustina, S., Bohigas, R. C., Merz, R., and Litz, L. 2002. Simulation of thermal building behaviour in modelica. In *Proceedings of the 2nd International Modelica Conference*, volume 154. Oberfpaffenhofen.

Fraisse, G., Viardot, C., Lafabrie, O., and Achard, G. 2002. Development of a simplified and accurate building model based on electrical analogy. *Energy and Buildings*, 34(10):1017–1031.

Lilis, G. N. 2012. SRC: A gbxml-based thermal and energy building simulation program. Lambert Academic Publishing.

Lilis, G. N., Giannakis, G. I., and Rovas, D. R. 2013. SRC and its applications to building thermal control. *Clima 2013,* accepted.

Neymark, J. et al. 2008. *International Energy Agency Building Energy Simulation Test and Diagnostic Method (IEA BESTEST): In-Depth Diagnostic Cases for Ground Coupled Heat Transfer Related to Slab-on-Grade Construction*. National Renewable Energy Laboratory.

Oppenheim, A. 1956. Radiation analysis by the network method. *Trans. ASME*, 78(4):725–735.

Perez, R., Ineichen, P., Seals, R., Michalsky, J., and Stewart, R. 1990. Modeling daylight availability and irradiance components from direct and global irradiance. *Solar energy*, 44(5):271–289.

Prívara, S., Cigler, J., Váňa, Z., Oldewurtel, F., Sagerschnig, C., and Žáčeková, E. 2012. Building modeling as a crucial part for building predictive control. *Energy and Buildings*.

Vatti, B.R. 1992. A generic solution to polygon clipping. *Communications of the ACM*, 35(7):56–63.

Winget, J.M. et. al. 1989. Improving radiosity solutions through the use of analytically determined form-factors. *Computer Graphics*, 23(3).